

# Spin rotations induced by electron running on closed trajectories in gated semiconductor nanodevices

S. Bednarek and B. Szafran  
*Faculty of Physics and Applied Computer Science,  
 AGH University of Science and Technology,  
 al. Mickiewicza 30, 30-059 Kraków, Poland*

A design for a quantum gate performing transformations of a single electron spin is presented. The spin rotations are performed by the electron going around the closed loops in a gated semiconductor device. We demonstrate the operation of NOT, phase-flip and Hadamard quantum gates, i.e. the single-qubit gates which are most commonly used in the algorithms. The proposed devices employ the self-focusing effect for the electron wave packet interacting with the electron gas on the electrodes and the Rashba spin-orbit coupling. Due to the self-focusing effect the electron moves in a compact wave packet. The spin-orbit coupling translates the spatial motion of the electron into the rotations of the spin. The device does not require microwave radiation and operates using low constant voltages. It is therefore suitable for selective single-spin rotations in larger registers.

PACS numbers: 73.21.La, 73.63.Nm, 03.67.Lx

Extensive work for design and construction of quantum processing devices is underway. The potential implementations are based on various effects and systems including photonic [1] and superconducting [2] devices, nuclear magnetic resonance [3] and ion traps [4]. In one of the approaches the quantum bits are stored by spins of electrons confined in semiconductor nanostructures [5]. Such a quantum gate can be naturally combined with a classical computer. So far the set-up and read-out [6] of the spin were realized as well as the spin rotations [7, 8, 9] in single and double dots.

According to the original proposal [5] a universal quantum gate requires exchange operations between pairs of spins combined with the single-spin rotations. The latter can be performed by the Rabi oscillations in an external microwave field. For a number of reasons selective single-spin rotations are considered more challenging to implement than the spin exchange between a pair of electrons [10]. The problem with the microwave radiation is that even at magnetic fields of the order of 10 T the spin Zeeman energy splitting is relatively low and the resonant wavelength is of the order of millimeters, which rather excludes fast and site-selective operations on a single spin without perturbing the others. It was therefore suggested that a universal two-qubit gate can be achieved applying the Heisenberg coupling only: employing additional registers [10], using inhomogenous Zeeman splitting [11] or exploiting the spin-orbit coupling [12]. Experimentally a site-selective single-spin rotations were eventually demonstrated with an embedded local microwave source [8] which however requires cooling of the heat generated by the AC currents. The cooling problem is avoided when the spin rotations are induced by oscillating electric fields [9] and occur due to the spin-orbit coupling. In this Letter we propose a device in which the single-spin operations are performed without the microwave radiation or fast voltage oscillations. The proposed device is based on

spatial motion of the confined electron in the presence of the spin-orbit coupling and requires application of low DC voltages only.

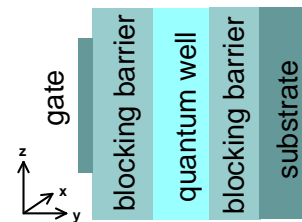


FIG. 1: (color online) Schematics of the consider semiconductor structure.

We recently showed that induced quantum wires and dots [13] are formed under metal gates deposited on a planar structure containing a quantum well due to the self-focusing effect [14, 15] for the wave function of the confined electron interacting with the electron gas in the metal. This effect assists in the 100% guaranteed transfer of a stable electron packet following a trajectory which is controlled by the gate set-up and applied DC voltages.

We consider a planar nanostructure of Fig. 1 with a quantum well and electrodes on top. A single electron is confined in the quantum well. We assume that the quantum well is made of a semiconductor of the diamond lattice structure (Si, Ge), in which the Dresselhaus spin-orbit coupling is absent due to the inversion symmetry of the crystal. The electron motion in the  $y$  direction is frozen by the quantum well confinement. We use a two-dimensional Hamiltonian

$$H(x, z, t) = -\frac{\hbar^2}{2m} \left( \frac{\partial^2}{\partial x^2} + \frac{\partial^2}{\partial z^2} \right) - e\phi_2(x, y_0, z, t) + H_R, \quad (1)$$

where  $y_0$  is the coordinate of the center of the quantum well and  $H_R$  is the Rashba spin-orbit coupling term

due to the asymmetry of the quantum well potential  $H_R = \alpha (p_z \sigma_x - p_x \sigma_z)$ , where  $p$  are the momentum operators and  $\sigma$ 's are the Pauli matrices. We write the state functions as vectors (spinors)

$$\Psi(x, z, t) = \begin{pmatrix} \psi_1(x, z, t) \\ \psi_2(x, z, t) \end{pmatrix}. \quad (2)$$

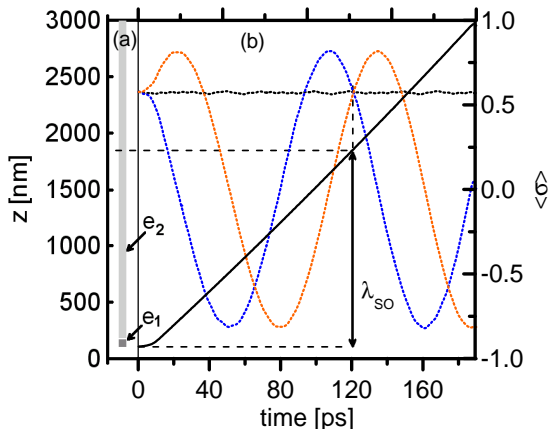


FIG. 2: (color online) (a) System of two electrodes ( $e_1, e_2$ ) on top of the structure. (b) Electron packet  $z$  position vs time (dark solid line, left axis). Dotted lines show average values of the Pauli operators:  $\langle \sigma_z \rangle$  (red color),  $\langle \sigma_x \rangle$  (black) and  $\langle \sigma_y \rangle$  (blue) and are referred to the right axis.

The electrostatic potential  $\phi_2$  of Eq. (1) is found from the Poisson equation using the methodology previously applied for simulations of electrostatic quantum dots [16].  $\phi_2$  is the difference of the total electrostatic potential  $\Phi$  and the electron self-interaction potential  $\phi_1$ ,  $\phi_2(\mathbf{r}, t) = \Phi(\mathbf{r}, t) - \phi_1(\mathbf{r}, t)$ . The total potential fulfills the 3D Poisson equation

$$\nabla^2 \Phi(\mathbf{r}, t) = -\rho(\mathbf{r}, t)/\epsilon\epsilon_0, \quad (3)$$

and the self-interaction potential is calculated with the Coulomb law

$$\phi_1(\mathbf{r}, t) = \frac{1}{4\pi\epsilon\epsilon_0} \int d\mathbf{r}' \frac{\rho(\mathbf{r}', t)}{|\mathbf{r} - \mathbf{r}'|}, \quad (4)$$

where  $\rho(\mathbf{r}, t)$  is the electron density calculated for wave function (2)

$$\rho(\mathbf{r}, t) = -e (|\psi_1(x, z, t)|^2 + |\psi_2(x, z, t)|^2) \delta(y - y_0). \quad (5)$$

Eq. (3) is solved numerically in a rectangular box containing the studied nanostructure. Potentials applied to the gates are assumed as Dirichlet boundary condition. The content of the computational box is charge neutral, so on its surface we assume vanishing normal component of the electric field. Calculated potential  $\phi_2(\mathbf{r}, t)$  contains a contribution of the charge induced on the metal surface by the confined electron. This contribution introduces the self-focusing effect [14]. The time dependence

in (3-5) enters due to the motion of the electron packet. As the initial condition we take the solution of a time-independent Schrödinger equation  $H(x, z)\Psi_0(x, z) = E\Psi_0(x, z)$  for a given spin-state. The time evolution is obtained numerically with a finite-difference scheme consistent with the time-dependent Schrödinger equation  $\Psi(t + dt) = \Psi(t - dt) - \frac{2i}{\hbar} H(t)\Psi(t)dt$ .

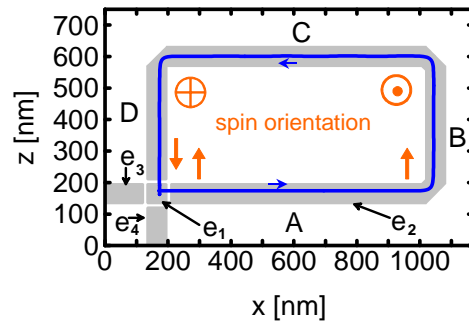


FIG. 3: (color online) Gate configuration (grey colors) for the NOT gate. Blue solid lines show the electron trajectory (electron starts from under  $e_1$  and goes to the right). Red symbols show the spin orientation near the corners of the trajectory ( $\odot, \oplus$  indicate ‘‘from the page’’ and ‘‘to the page’’ directions, respectively).

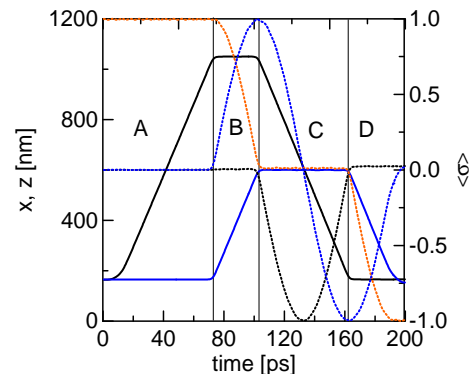


FIG. 4: (color online) Same as Fig. 2 but for the NOT gate of Fig. 3. The black (blue) solid curves show the  $x, (z)$  positions as a function of time.

Applying weak voltages to the gates with respect to the substrate one can [13] set the electron packet in motion and stop it in a chosen location. The products of the momentum and spin operators in the  $H_R$  operator perturb somewhat the electron trajectories. Electron motion influences the spin in a much more pronounced extent.

Let us consider the system presented in Fig. 2(a) with two electrodes  $e_1$  and  $e_2$  placed parallel to the  $z$  axis on top of the structure of Fig. 1. In the initial state we put zero voltage to electrode  $e_1$  and small negative to  $e_2$  [13]. The ground-state wave function is formed under  $e_1$ . We assume that the spin is in the state which has the same average value in all  $x, y, z$  directions,

$\Psi(x, z, 0) = \Psi_0(x, z) \frac{1}{\sqrt{2}\sqrt{\sqrt{3}+3}} \begin{bmatrix} (1 + \sqrt{3}) \\ (1 + i) \end{bmatrix}$ . The motion of the packet starts when the voltage applied to  $e_2$  is switched to  $V_2 = 0.2$  mV which extracts the electron from underneath the gate  $e_1$ . The electron is initially accelerated when it passes from under  $e_1$  to under  $e_2$ , then it moves with a constant velocity. The time dependence of the electron position is given in Fig. 2(b) with a solid black line. The dotted curves show the average values of the components of the spin. We see that for the electron moving parallel to the  $z$  axis the  $\langle \sigma_x \rangle$  value is preserved and the  $\langle \sigma_y \rangle$  and  $\langle \sigma_z \rangle$  components oscillate: the spin is rotated around the  $x$  axis. Similarly, for the electron moving along the  $z$  direction the Rashba coupling leads to the spin rotation around the  $x$  axis. The rotation angle depends on the coupling constants, the electron effective mass, and the distance traveled by the electron. For simulations presented in Fig. 3 we assume the coupling constant  $\alpha = 7.2 \times 10^{-13}$  eVnm within the range predicted for the asymmetric quantum wells [17]. The quantum well and the potential barriers are taken 10 nm thick. We apply the Si material parameters  $m = 0.19m_0$  and  $\epsilon = 13$ . We deduce that the distance for which the initial spin is restored is  $\lambda_{SO} = 1.8 \mu\text{m}$ .

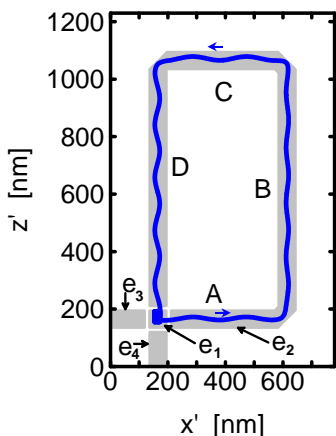


FIG. 5: (color online) Gate configuration (grey colors) for the Hadamard gate. Blue solid lines show the electron trajectory (electron starts from under  $e_1$  and goes to the right – the direction of motion is marked with the blue arrows). The rectangular gate path is rotated by  $45^\circ$  with respect to Fig. 3:  $z' = \frac{1}{\sqrt{2}}(x + z)$ ,  $x' = \frac{1}{\sqrt{2}}(x - z)$ .

Since the electron motion along perpendicular directions induces spin rotations around perpendicular axes, one can perform any rotation by making the electron move under electrodes forming a closed loop. In Fig. 3 we propose a setup performing the logical NOT operation on the electron spin. The electrodes are marked with the grey color. The spin of the electron confined in the quantum dot induced [13] under  $e_1$  electrode stores the qubit. The  $e_2$  electrode serves to guide the electron

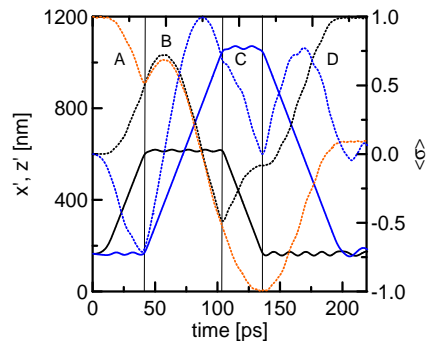


FIG. 6: (color online) Position of the electron packet as a function of time for the Hadamard gate of Fig. 5 in the rotated system of coordinates  $(x', y', z')$ . The black (blue) solid curves show the  $x'$ , ( $z'$ ) positions. The dotted curves show the expectation value of the Pauli matrix operators defined with respect to the  $x, y, z$  axes.

around a closed loop back to the dot induced under  $e_1$ . For illustration initially the  $z$ -component of the spin is set in the “up” state  $\Psi(x, z, 0) = \begin{pmatrix} \Psi_0(x, z) \\ 0 \end{pmatrix}$ . The packet is set in motion to the right by applying a constant  $+0.2$  mV voltage to  $e_2$  and a short pulse of  $-0.4$  mV to  $e_3$ . The electron trajectory is drawn with the blue curve in Fig. 3. The time dependence of the electron position is plotted in Fig. 4 (black curve shows the  $x$  position and the blue one the  $z$  position). In the A region we notice an initial increase of the velocity and then a constant velocity motion till the end of the A segment. After reflection at the cut corner [13] the electron goes into the B part where the  $x$  position becomes fixed and the  $z$  one increases with time. Passing under the C segment the electron returns to its initial  $x$  coordinate and under the D segment to its initial  $z$  coordinate. At the end of the electron slows down which results of the  $e_1, e_2$  potential difference. When the electron comes to under  $e_1$  the potential of this electrode is changed to  $+0.3$  meV which traps the electron in the induced dot. The oscillations of the blue curve at the end of the motion are due to an excess of the kinetic energy.

The spin direction at the corners of the loop is schematically marked by arrows in Fig. 3. The time dependence of  $\langle \sigma_x \rangle$ ,  $\langle \sigma_y \rangle$  and  $\langle \sigma_z \rangle$  are plotted in Fig. 4 with dotted lines: black, blue and red, respectively. Initially the spin is oriented “up”  $\langle \sigma_z \rangle = 1$ , and  $\langle \sigma_x \rangle = \langle \sigma_y \rangle = 0$ . In the A segment the electron moves in the  $x$  direction so the spin is rotated around the  $z$  axis and no spin change is observed in Fig. 4. The length of the B segment is such that the spin is rotated around the  $z$  axis by  $90^\circ$  and takes the “from the page” orientation: the spin is in the  $\sigma_y$  eigenstate and  $\langle \sigma_y \rangle = 1$ . When the electron returns in the  $-x$  direction the spin is rotated by  $180^\circ$  degrees and takes the “to the page” orientation  $\langle \sigma_y \rangle = -1$  at

the end of the  $C$  part. On the  $D$  segment the spin is rotated by  $-90^\circ$  degrees around the  $x$  axis. Returning to  $e_1$  the electron is in the “down” spin eigenstate  $\langle\sigma_z\rangle = -1$ . Similarly one can show that the same trajectory inverts the spin of initial “down” orientation. Thus the motion around the loop performs the NOT operation

$$U^{\text{NOT}} = \begin{pmatrix} 0 & 1 \\ 1 & 0 \end{pmatrix}. \quad (6)$$

In the theory of quantum computation other useful single qubit operations are the Hadamard transformation  $U^H$  of the basis states into their equilibrated superpositions and the phase flip operation  $U^\pi$

$$U^H = \frac{1}{\sqrt{2}} \begin{pmatrix} 1 & 1 \\ 1 & -1 \end{pmatrix}, U^\pi = \frac{1}{\sqrt{2}} \begin{pmatrix} 1 & 0 \\ 0 & -1 \end{pmatrix}. \quad (7)$$

The loop of Fig. 3 can be used as the Hadamard gate for the spin “up” and “down” states redefined with respect to the direction bisecting the angle between  $x$  and  $-z$  axes. Alternatively one can keep the basis set and rotate the electron trajectory (the electrode loop) by 45 degrees in the  $(x, z)$  plane. The electrode system corresponding to this gate and the electron trajectory are depicted in Fig. 5. The plot is drawn in rotated coordinate system  $z' = \frac{1}{\sqrt{2}}(x+z)$ ,  $x' = \frac{1}{\sqrt{2}}(x-z)$ . The simulation of the Hadamard gate operation was performed similarly as the one performing the NOT operation. As the initial condition we took the electron confined below the  $e_1$  electrode in the ground-state with the spin parallel to the  $z$  axis. The packet is set in motion to the right by introducing a potential difference between  $e_1$  and  $e_2$  equal to  $-0.2$  mV. This time one cannot illustrate the spin orientation near the corners of the trajectory because the rotation angles are not multiples of  $90^\circ$  and in two first corners the spin projections on the  $x, y, z$  axes are not definite. This can be clearly seen in Fig. 6 which shows the time dependence of the spin average values. The spin initially oriented “up”  $\langle\sigma_z\rangle = 1$ , after closing the trajectory loop is set to the “right”  $\langle\sigma_x\rangle = 1$ . Similarly, the spin “down”  $\langle\sigma_z\rangle = -1$  turns to the “left” at the end of the loop. Twofold rotation around the loop is equivalent to the identity transform, i.e. the rotation by the full angle.

The phase-shift operation  $U^\pi$  is performed by the electrode configuration rotated by a  $90^\circ$  angle with respect to the NOT gate of Fig. 3. The NOT quantum gate oriented as in Fig. 3 performs the  $U^\pi$  transformation for the “up” and “down” states redefined as parallel and antiparallel to the  $x$  axis.

The devices proposed here use the Rashba coupling in the absence of the Dresselhaus interaction. These devices can be realized in semiconductors of the diamond

lattice (Si, Ge). The Rashba coupling can be tuned by external electric field and it becomes arbitrarily small for nearly symmetric quantum wells. For devices based on zinc blende materials (III-V’s or II-VI’s) one cannot get rid of the Dresselhaus term but one can still design electron trajectories performing the spin operations for both couplings present [18].

We demonstrated that the controlled electron motion around closed loops along induced quantum wires combined with the spin-orbit coupling can be used to design devices performing any single-spin rotation. The proposed device is scalable and since it runs without a microwave radiation or high frequency electric fields it offers an independent control of many separate qubits.

- 
- [1] J.L. O’Brien *et al.* Nature **426**, 264 (2003).
  - [2] Y. Nakamura, Yu. A. Pashkin, and J. S. Tsai, Nature **398**, 786 (1999).
  - [3] L.M.K. Vandersypen *et al.*, Nature **414**, 883 (2001).
  - [4] D. J. Wineland *et al.*, J. Res. Natl. Inst. Stand. Technol. **103**, 259 (1998).
  - [5] D. Loss and D. P. DiVincenzo, Phys. Rev. A **57**, 120 (1998); D. Awschalom, D. Loss, and N. Samarth, *Semiconductor Spintronics and Quantum Computation*, Springer Verlag, Berlin, (2002); R. Hanson *et al.*, Rev. Mod. Phys. **79**, 1217 (2007).
  - [6] J. M. Elzermann *et al.*, Nature **430**, 431 (2004); R. Hanson *et al.*, Phys. Rev. Lett. **94**, 196802 (2005); T. Meunier *et al.*, Phys. Rev. B **74**, 195303 (2006).
  - [7] J. R. Petta *et al.*, Science **309**, 2180 (2005); F.H.L. Koppens *et al.*, Nature **442**, 766 (2006). W. A. Colsh and D. Loss, Phys. Rev. B **75**, 161302 (2007).
  - [8] F. H. L. Koppens *et al.*, Nature **442**, 766 (2006).
  - [9] K.C. Nowack *et al.*, Science **318**, 1430 (2007).
  - [10] D. P. DiVincenzo *et al.*, Nature **408**, 339 (2000).
  - [11] J. Levy, Phys. Rev. Lett. **89**, 147902 (2002).
  - [12] D. Stepanenko and N.E. Bonesteel, Phys. Rev. Lett. **94**, 140501 (2004).
  - [13] S. Bednarek, B. Szafran, R. J. Dudek and K. Lis, Phys. Rev. Lett. **100**, 126805 (2008).
  - [14] S. Bednarek, B. Szafran, and K. Lis, Phys. Rev. B **72**, 075319 (2005).
  - [15] S. Bednarek and B. Szafran, Phys. Rev. B **73**, 155318 (2006).
  - [16] S. Bednarek, B. Szafran, and J. Adamowski, Phys. Rev. B **61**, 4461 (2000); **64**, 195303 (2001); S. Bednarek, B. Szafran, K. Lis, and J. Adamowski, Phys. Rev. B **68**, 155333 (2003); S. Bednarek, K. Lis, and B. Szafran, Phys. Rev. B **77**, 115320 (2008).
  - [17] E.A. de Andrada e Silva, G.C. La Rocca, and F. Bassani, Phys. Rev. B **55**, 16293 (1997).
  - [18] S. Bednarek, in preparation.